FORMATION OF NANOCRYSTALLINE ALUMINUM MAGNESIUM ALLOYS BY MECHANICAL ALLOYING

J. GUBICZA[a,c], M. KASSEM[b] and T. UNGÁR[c]

[a]Dept. of Solid State Physics, Eötvös Univ., Budapest, P.O.Box 32, H-1518, Hungary
[b]Dept. of Materials Sci. and Eng., Faculty of Pet. and Mining, Suez Canal Univ., Suez, Egypt, mkassem54@yahoo.com
[c]Dept. of General Physics, Eötvös University, Budapest, P.O.Box 32, H-1518, Hungary

ABSTRACT

The effect of the nominal Mg content and the milling time on the microstructure and the hardness of mechanically alloyed Al (Mg) solid solutions is studied. The crystallite size distribution and the dislocation structure are determined by X-ray diffraction peak profile analysis and the hardness is obtained from depth sensing indentation test. Magnesium gradually goes into solid solution during ball milling and after about 3 h almost complete solid solution state is attained up to the nominal Mg content of the alloys. With increasing milling time the dislocation density, the hardness and the Mg content in solid solution are increasing, whereas the crystallite size is decreasing. A similar tendency of these parameters is observed at a particular duration of ball milling with increasing of the nominal Mg content. At the same time for long milling period the dislocation density slightly decreases together with a slight reduction of the hardness.

Keywords: Al-Mg Alloys, Mechanical Alloying, X-Ray Peak Profile Analysis, Crystallite Size, Dislocation Structure, Hardness.

1. INTRODUCTION

Mechanical alloying (MA) is an effective tool to produce metal alloys with fine microstructure. During the process the particles of the initial powders are deformed heavily and repeatedly by high energy milling and the atoms of the additions are soluted

into the matrix of the main component. Ball milling is employed to obtain alloys with extended solubilities, dispersion-hardened metals, nanocrystalline and amorphous materials [1,2]. The ball milling-induced amorphization requires very high ball-to-powder ratio and moderate rotation speed since the friction and the sliding between the outer balls and the inner wall of the vial are the major events in amorphization [2]. At the same time in the production of crystalline alloys by MA the main mechanisms are the impact and the collision between the balls and the powder. During ball milling two essential processes occure: cold welding between the different particles and fracturing of the cold welded particles due to high energy collision [1]. The cold welding minimizes the diffusion distance between the different atoms. The fracturing of the welded particles impedes the clustering of the particles promoting the transfer of the high ball collision energy to all particles and produces new, clean surfaces without oxide layers accelerating the diffusion [1]. The reaction kinetics of MA has been investigated experimentally by Schaeffer and Forrester [3]. They found that the strain accumulation rate and the reaction rate increased rapidly with the density of the balls, i.e. the collision energy [3]. Models are also developed for describing the MA process and to predict the changes in the powder properties [4]. Using model calculations and computer simulations Huang and coworkers studied the dynamics of a vibratory mill [5]. The effect of the system dynamics on the microstructural evolution of the powder has been also investigated experimentally and it was shown that in a vibratory mill the impact force can be used for the characterization of the microstructural evolution of the milled powder [5].

X-ray diffraction (XRD) is often used for the determination of microstructure of crystalline materials. X-ray diffraction line profiles are broadened due to the smallness of crystallites and lattice distortions. The two effects can be separated on the basis of the different diffraction order dependence of peak broadening. The standard methods of X-ray diffraction profile analysis based on the full widths at half maximum (FWHM), the integral breadths and on the Fourier coefficients of the profiles provide the apparent crystallite size and the mean square strain [6-8]. If the shape of the crystallites can be assumed to be uniform, a crystallite size distribution function having two free parameters can be also determined [9-13]. The evaluation of the X-ray profiles is further complicated by the anisotropic strain broadening of the diffraction lines. This means that neither the full width at half maximum nor the integral breadth nor the Fourier coefficients of the profiles are monotonous functions of the diffraction vector [14-16]. It has been shown recently that the strain anisotropy can be well accounted for by the dislocation model of the mean square strain by introducing the contrast factors of dislocations [17-22]. Since the values of the dislocation contrast factors depend on the type of dislocations present in the crystal, the evaluation of X-ray profiles for the contrast factors enables the determination of the dislocation structure.

An evaluation procedure of X-ray diffraction profiles was elaborated recently for the determination of the crystallite size distribution and the dislocation structure in nanocrystalline materials [23-24]. In this method the Fourier coefficients of the

measured physical profiles are fitted by the Fourier coefficients of well established *ab initio* functions of size and strain profiles. The fitting procedure gives the median and the variance of the size distribution of crystallites, the density and the arrangement parameter of dislocations and one parameter for the character (edge or screw) of dislocations.

In this paper the microstructure of nanocrystalline Al-Mg alloys produced by ball milling of Al and Mg powders are investigated by X-ray diffraction profile analysis. The crystallite size distribution and the dislocation structure are determined and the hardness of the compacted powders is also measured as a function of the Mg content and the milling time. It is shown that by ball milling the two components are mechanically alloyed beyond the equilibrium solubility limit at room temperature (RT) with a very fine nano-size microstructure.

2. EXPERIMENTAL

A series of aluminum-magnesium samples were prepared from high purity aluminum (99.9%) powder and high purity magnesium chips (less than 2mm. thick and 5mm long). The mechanical alloying was carried using a Spex8000 shaker miller at room temperature. The charge was loaded into a steel vial in a glove box with a purified argon (<3ppm oxygen) atmosphere. Martensitic stainless steel (440C) balls with the diameters of 6.4 mm and 7.9 mm were used for milling where the ball to powder ratio was 10:1. Stearic acid (2%) was used as a control agent to prevent severe cold welding. Aluminum with 6wt% magnesium alloys were milled for up to 6 hours. A series of Al − x wt% Mg (x=0, 3, 6) were milled for 3 hours at the same conditions to study the effect of Mg concentration. The milled powders were compacted with the pressure of 1 GPa and the surface of the compacted specimens were polished carefully for hardness measurements.

The hardness was studied by Depth Sensing Indentation test (DSI) [25]. The DSI measurements were carried out by a Shimadzu-made dynamic ultra-micro hardness tester (DUH 202). Each DSI test consisted of a loading-unloading cycle. During the loading period a Vickers indenter penetrated into the surface of the sample at constant loading rate (2.65 mN/s) and the same rate was applied in the unloading period when the pyramid moved backwards. The maximum load in each test was 100 mN.

The microstructure of both the ball-milled powders and the compacted specimens were studied by X-ray diffraction profile analysis. The diffraction profiles were measured by a Philips X'pert diffractometer using Cu anode and pyrolithic graphite secondary monochromator. The step size and the step time were 0.03^0 and 22 seconds/step, respectively. The instrumental corrections were made by using the powder pattern of a Si standard (NBS 640a) and the usual Stokes correction procedure.

3. EVALUATION OF THE X-RAY DIFFRACTION PROFILES

According to the kinematical theory of X-ray diffraction, the physical profile of a Bragg reflection is given by the convolution of the size and the distortion profiles while the Fourier transform of the physical diffraction profile is given as the product of the size and the distortion Fourier coefficients, A^S and A^D [7]. Assuming that in the crystal the lattice distortions are caused by dislocations [17-19]

$$A^D (L) = \exp[- \rho B L^2 f(\eta) \, g^2 \overline{C}], \tag{1}$$

where L is the Fourier variable, $B=\pi b^2/2$, b is the absolute value of the Burgers vector, ρ is the dislocation density, $\eta \sim L/R_e$, R_e is the effective outer cut-off radius of dislocations, g is the absolute value of the diffraction vector, $\overline{C}$ is the average dislocation contrast factor and $f(\eta)$ is a function derived explicitly by Wilkens (see Eqs. A.6 to A.8 in Ref. [19] and Eqs. (22) and (23) in Ref. [23]). Instead of R_e, it is physically more appropriate to use the parameter $M= R_e \sqrt{\rho}$ defined by Wilkens as the dislocation arrangement parameter [19]. The value of M gives the strength of the dipole character of dislocations: the higher the value of M, the weaker the dipole character and the screening of the displacement fields of dislocations.

The average dislocation contrast factors are the weighted average of the individual C factors either over the dislocation population or over the permutations of the *hkl* indices [26-28]. Based on the theory of line broadening caused by dislocations, it can been shown that in an untextured cubic polycrystalline specimen the values of $\overline{C}$ are simple functions of the invariants of the fourth order polynomials of *hkl* [28]

$$\overline{C} = \overline{C}_{h00} \{1 - q(h^2k^2 + h^2l^2 + k^2l^2)/(h^2+k^2+l^2)^2\}, \tag{2}$$

where $\overline{C}_{h00}$ is the average dislocation contrast factor for the *h00* reflections and q is a parameter depending on the elastic constants of the crystal and on the character of dislocations (e.g. edge or screw type).

It was observed by many authors that in powder or bulk nanocrystalline specimens the crystallite-size distribution can be described by log-normal function [9,10,13,29,30]

$$f(x) = \frac{1}{\sqrt{2\pi}\,\sigma}\frac{1}{x}\exp\left\{-\frac{[\ln(x/m)]^2}{2\sigma^2}\right\}, \tag{3}$$

where x is the crystallite size (the diameter of the crystallites), σ is the variance and m is the median of the size distribution function $f(x)$. For spherical crystallites with log-normal size distribution, the arithmetically, the area- and the volume-weighted mean crystallite sizes are obtained as [31]

$$<x>_{arit} = m \exp(0.5\ \sigma^2). \tag{4}$$

$$<x>_{area} = m \exp(2.5\ \sigma^2). \tag{5}$$

$$<x>_{vol} = m \exp(3.5\ \sigma^2). \tag{6}$$

Assuming spherical crystallite shape with log-normal size distribution, the Fourier transform of the size profile can be given as:

$$A^S(L) \sim \frac{m^3 \exp(4.5\sigma^2)}{3} erfc\left[\frac{\ln(|L|/m)}{\sqrt{2}\ \sigma} - 1.5\sqrt{2}\sigma\right] -$$
$$- \frac{m^2 \exp(2\sigma^2)|L|}{2} erfc\left[\frac{\ln(|L|/m)}{\sqrt{2}\ \sigma} - \sqrt{2}\sigma\right] + \frac{|L|^3}{6} erfc\left[\frac{\ln(|L|/m)}{\sqrt{2}\ \sigma}\right]. \tag{7}$$

where *erfc* is the complementary error function.

A numerical procedure has been worked out for fitting the Fourier transform of the experimental profiles by the product of the theoretical functions of size and strain Fourier transforms given in Eqs. 1 and 7 [23,24]. The method has the following steps: i) the Fourier coefficients of the experimental profiles have been calculated by a non-equidistant sampling Fourier transformation, ii) the instrumental correction was carried out by the Stokes method [32] using Si standard (NBS 640), iii) the Fourier coefficients of the size and strain profiles were calculated by using Eqs. 1, 2 and 4, (iv) the corrected experimental and the calculated Fourier coefficients were compared by the least squares method. The procedure has five fitting parameters for cubic crystals: (i) *m* and (ii) σ of the log-normal size distribution function, (iii) ρ, (iv) *M* and (v) *q* characterising the dislocation structure. Further details of the fitting procedure are given elsewhere [24].

4. RESULTS AND DISCUSSION

For Al - 6wt% Mg powders milled for 0.5 and 6 h the parts of the X-ray diffractograms corresponding to 2Θ region between 30 and 53^0 are plotted in Figs. 1.a and 1.b, respectively. The most intense Mg peaks were clearly visible in Fig. 1.a and they disappeared gradually during ball milling. After 6 h ball milling the Mg peaks almost completely disappeared (see Fig. 1.b) which corresponds to the dissolution of Mg atoms into the Al matrix. The lattice constants of Al-Mg alloys produced by mechanical alloying were determined from the positions of the X-ray diffraction peaks. The Mg content of Al solid solutions was obtained by adjusting the measured lattice constants to the Vegard's plot of Pool and Axon [33] which is shown in Fig. 2. The lattice constants
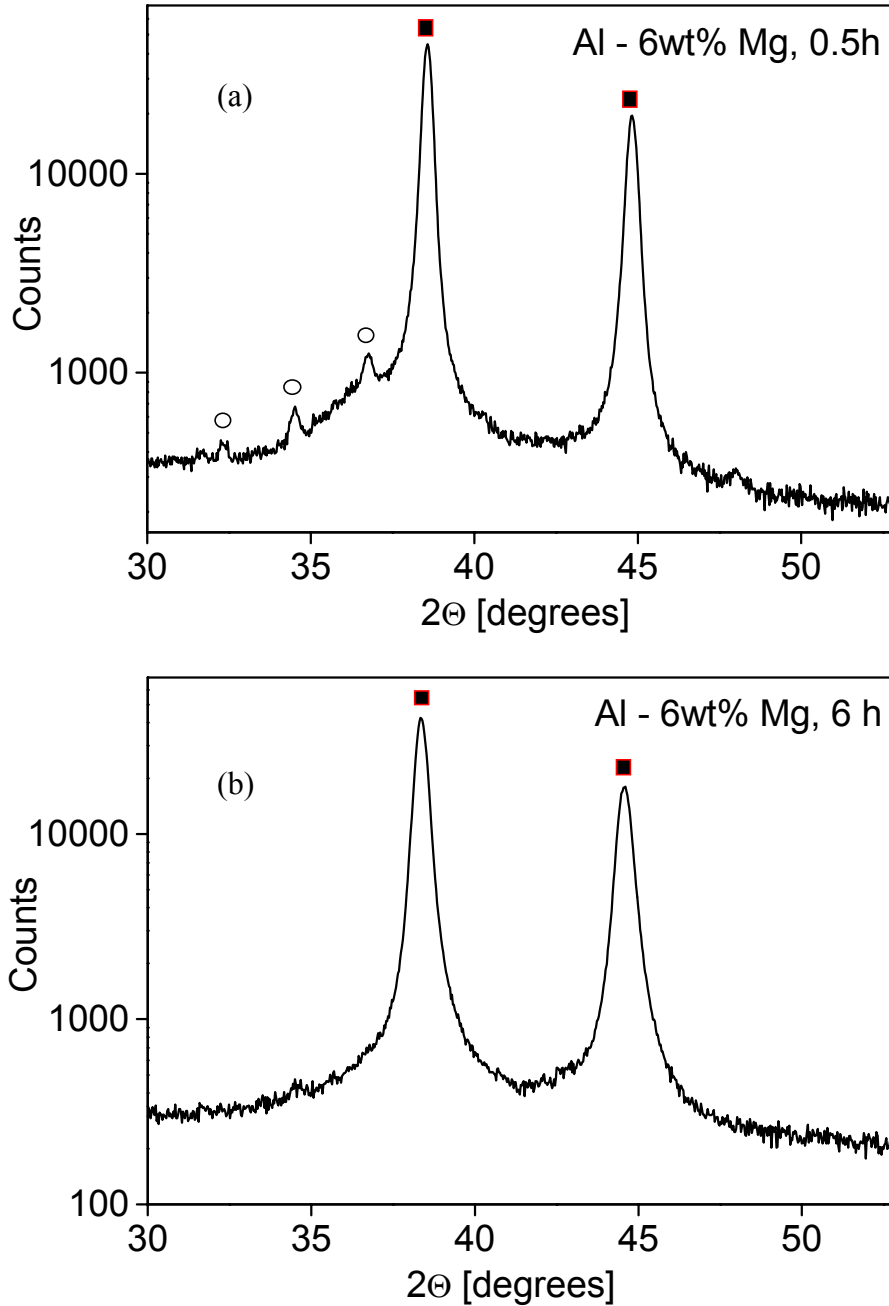
Fig. 1. The parts of the X-ray diffractograms corresponding to 2Θ region between 30 and 53^0 for Al - 6wt% Mg powders milled for 0.5 (a) and 6 h (b). The solid squares and the open circles represent the peaks of Al and Mg, respectively.

and the Mg concentration are listed in Table 1.a and 1.b for Al - 6wt% Mg powder mixtures milled for different time up to 6 h and for powders with different nominal Mg content milled for 3 h, respectively. As can be seen the Mg concentration in Al alloys is increasing with the milling time for a particular powder mixture composition and also
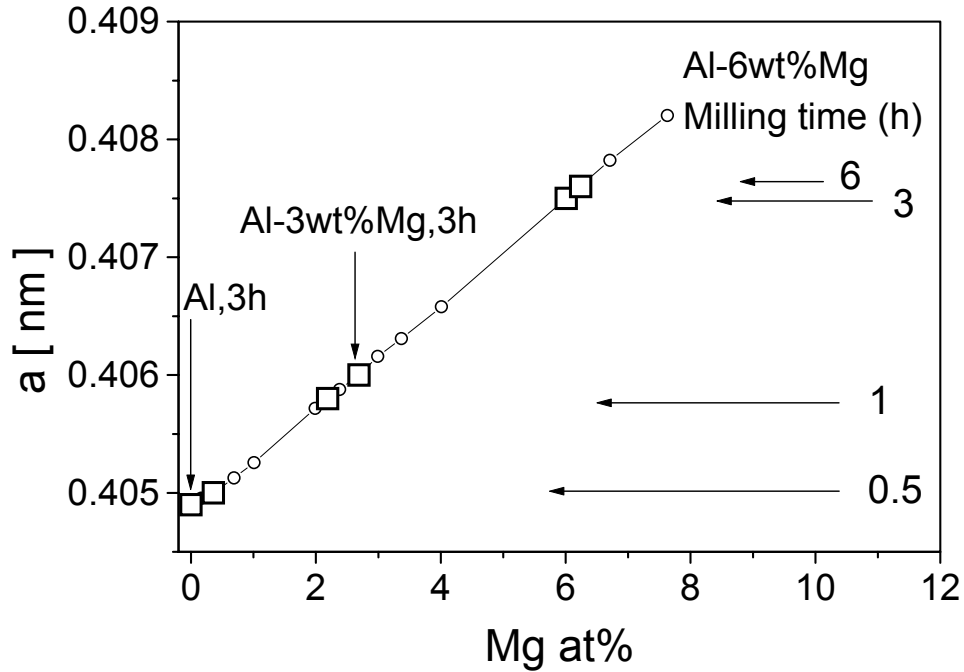
Fig. 2. The lattice constant vs Mg concentration in Al lattice (the Vegard's plot of Pool and Axon [33]). The measured lattice constants corresponding to the ball milled specimens are represented by open squares.

with the Mg content of the powders for a particular milling time. The equilibrium solubility limit of Mg in Al at room temperature is about 3at% [34,35] which is well exceeded up to about 6at%, by mechanical alloying as it can be seen in Fig. 2.

Table 1.a. The lattice parameter (a), the calculated Mg content and the microstructural parameters determined from X-ray diffraction for the powder mixture of the nominal composition Al - 6wt% Mg with different milling time.

Milling time [h]	a [nm]	Mg [wt%]	m [nm]	σ	$<x>_{vol}$ [nm]	$\rho\ 10^{14}$ [m^{-2}]	M	q
0.5	0.4050	0.32	29	0.36	46	12	1.5	0.91
1	0.4058	1.98	16	0.41	29	36	2.4	0.42
3	0.4075	5.44	19	0.38	31	44	2.0	0.37
6	0.4076	5.65	17	0.40	30	32	1.63	0.90

Table 1.b. The lattice parameter (a), the calculated Mg content and the microstructural parameters determined from X-ray diffraction for the powders with different nominal Mg content milled for 3 h.

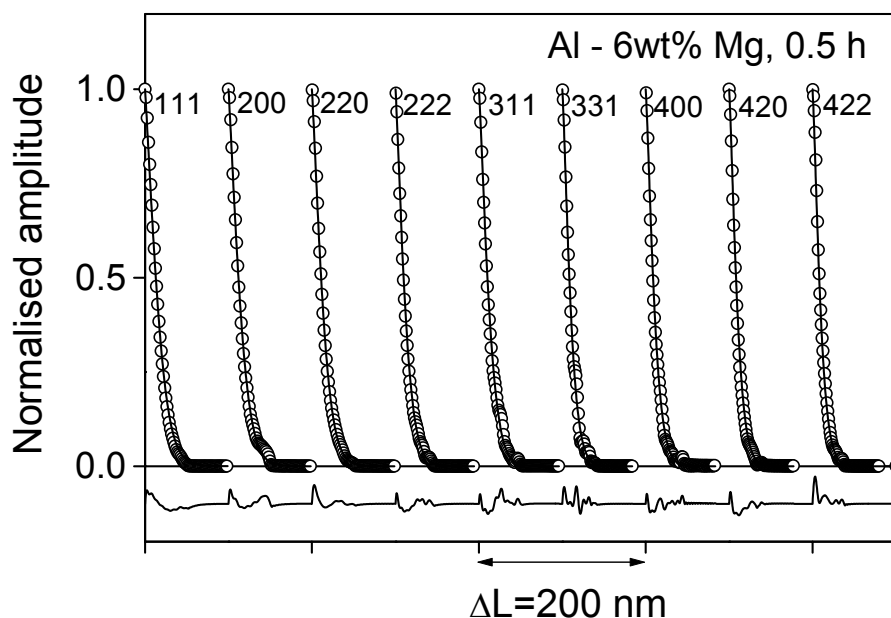| Nominal Mg [wt%]	a [nm]	Mg [wt%]	m [nm]	σ	$<x>_{vol}$ [nm]	$\rho\ 10^{14}$ [m^{-2}]	M	q
0	0.4049	0.00	56	0.19	64	9	1.0	1.17
3	0.4060	2.43	33	0.24	40	25	2.0	0.75
6	0.4075	5.44	19	0.38	31	44	2.0	0.37

Fig. 3. The measured and the fitted Fourier transforms for the specimen produced from Al - 6wt% Mg powder mixture milled for 0.5 h. The difference between the measured and the fitted values is also plotted in the lower part of the figure. The scaling of the differences is the same as in the main part of the figure.

The microstructural parameters of Al alloys were determined from the X-ray diffraction profiles by the procedure described in Section 3. The measured and the fitted Fourier transforms are shown in Fig. 3 for the specimen produced from Al - 6wt% Mg powder mixture milled for 0.5 h. The difference between the measured and the fitted values is also plotted in the lower part of the figure. The scaling of the differences is the same as in the main part of the figure. The agreement between the measured and the fitted Fourier transforms is very good. The microstructural parameters obtained from the fitting procedure are listed in Tables 1.a and 1.b. The relative uncertainties of these parameters are between 10-15 %. The volume-weighted crystallite size, the dislocation density and the Mg concentration as a function of the milling time and the nominal Mg content are plotted in Figs. 4 and 5, respectively. For the Al - 6wt% Mg samples the Mg concentration, the dislocation density increased while the crystallite size decreased rapidly with milling time up to 3 h. Between 3 and 6 h the Mg concentration and the crystallite size did not change significantly while the dislocation density sligthly decreased (Fig. 4). The decrease of the dislocation density or the strain in the crystal lattice between 3 and 6 h is reflected in that the diffraction peaks of Al - 6wt% Mg (6h) specimen are narrower than those of the Al - 6wt% Mg (3h) sample. The 200 reflections of the above two specimens are shown in Fig. 6. Lu et al. have obtained similar value for the crystallite size (20-30 nm) in Al - 37wt% Mg after 5 h ball milling [1]. The decreasing of the crystallite size and the increasing of the dislocation density with the milling time are in good agreement with results obtained for pure Al by Révész et al. [36]. At the same time the
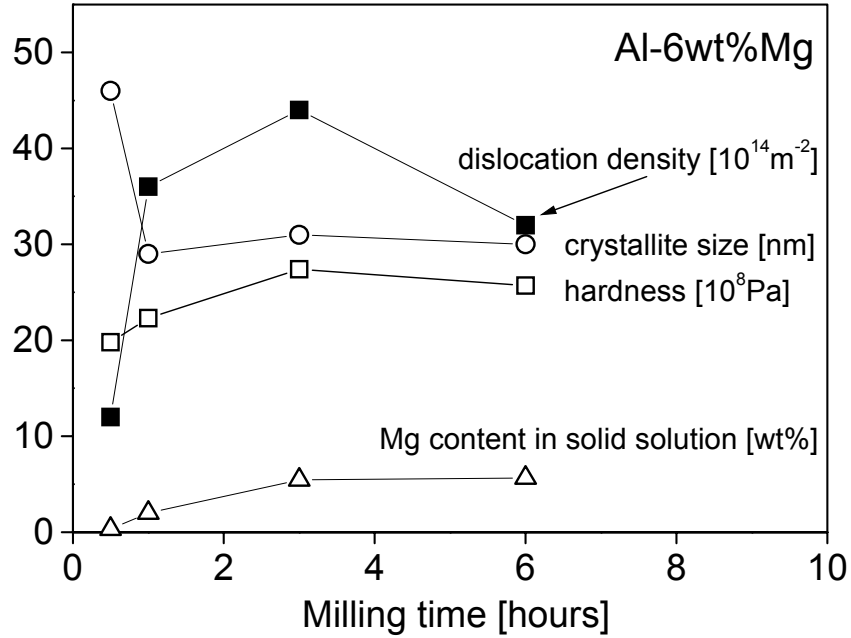
Fig. 4. The volume-weighted crystallite size, the dislocation density, the Mg concentration and the hardness as a function of the milling time for the specimen with the nominal Al - 6wt%Mg composition.
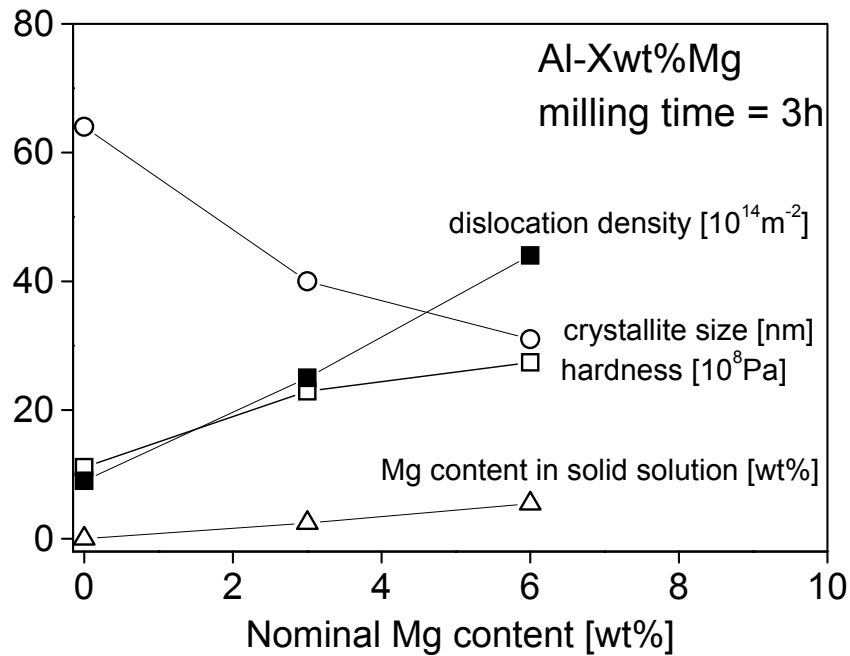

Fig. 5. The volume-weighted crystallite size, the dislocation density, the Mg concentration and the hardness as a function of the nominal Mg content for the specimens milled for 3 h.
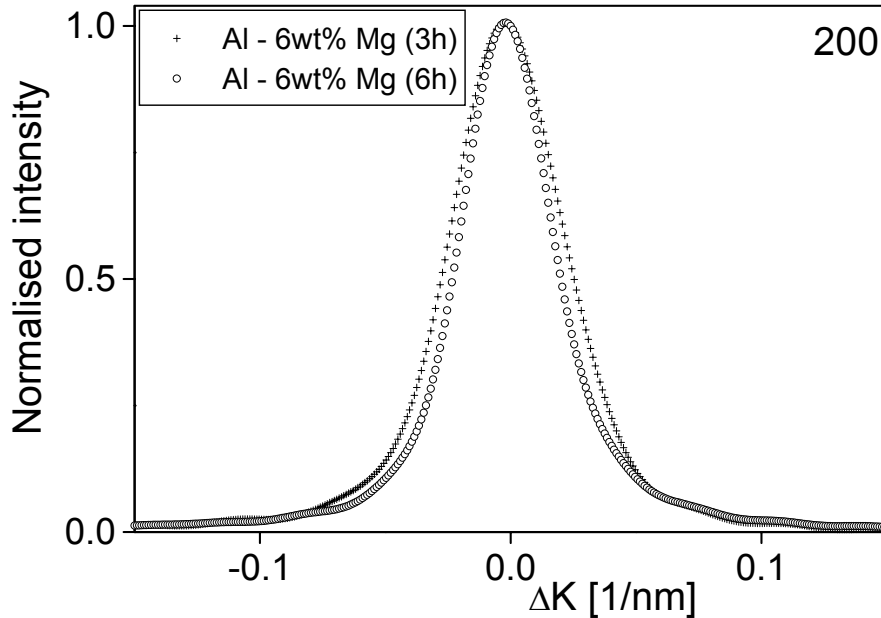
Fig. 6. The diffraction profiles of the 200 reflection for Al - 6wt% Mg (3h) and Al - 6wt% Mg (6h) specimens.

decreasing of the dislocation density in pure Al has been not observed in spite of the long milling time (32 days). For the powders milled for 3 h the Mg concentration and the dislocation density increased whilst the crystallite size decreased with the nominal Mg content (Fig. 5).

The character of dislocations can be monitored by using the parameter q. In a previous work, the values of q have been calculated for aluminium using the elastic constants given by Hearmon [37] and assuming the most common dislocation slip system with the Burgers vector $\mathbf{b}$=a/2<110>{111} [27]. It was found that for pure screw or pure edge dislocations the values of q are 1.33 or 0.36, respectively. The parameters q obtained for the ball milled Al alloys are listed in Tables 1.a and 1.b. For the alloy milled for 0.5 h the value of q is 0.91 which means that the character of dislocations is half edge - half screw (mixed). With increasing milling time the character of dislocations is shifted to more edge type, however after 6 h milling the character is mixed again. For pure Al milled for 3 h the character of dislocations is more screw type. With increasing Mg content the dislocation character became gradually more edge type. The dislocation structure and its thermal stability in Al-Mg alloys has been extensively studied in a number of earlier works [38-42]. Based on transmission electron microscopy (TEM) it was claimed that during cold rolling the dislocation structure in Al-Mg alloys, in a similar way as in pure Al, is rearranged for minimising its energy, calling these arrangements low-energy-dislocation-structures, LEDS [39,40]. The rearrangement of dislocations is, however, influenced by the strong interaction between solute Mg atoms and dislocations which is a large constraint on the dislocation mobility [39,40]. In cold-

rolled Al - 2.5wt% Mg alloys calorimetry measurements showed that the recovery of the microstructure proceeds after the oversize Mg atoms break away from the core of the dislocations [38]. As shown above, up to 3 h ball milling the dislocation density increases while its character shifts toward edge type. At the same time the arrangement parameter, *M*, remains relatively high, indicating that the dipole character remains weak. In this stage of MA the microstructure evolution resembles the formation of LEDS, however, this is somewhat contradicted by the increase of the total dislocation density and the weak dipole character, most probably due to the pinning effect of solute Mg atoms. During further ball milling the total dislocation density decreses and the character shifts toward mixed edge and screw. This process could be due to dynamic recovery induced by large plastic deformation and/or some temperature raise during ball milling.

For hardness measurements the ball milled powders were compacted. To check the effect of compaction on the microstructure, the parameters of the crystallite size distribution and the dislocation structure of the compacted specimens were determined by X-ray diffraction profile analysis. The results are shown for Al - 6wt% Mg samples with different milling time in Table 2.a and for the specimens milled for 3 h with different nominal Mg content in Table 2.b. Comparing the microstructural parameters obtained before and after compaction one can conclude that this procedure has only slight effect on the microstructure of the ball milled specimens, so that the hardness measured on the compacted samples characterizes the mechanical behaviour of the milled Al alloys.

Table 2.a. The microstructural parameters and the hardness for the specimens compacted from the powder mixture of the nominal composition Al - 6wt% Mg after ball milling for different time.

Milling time [h]	m [nm]	σ	$\langle x \rangle_{vol}$ [nm]	ρ 10^{14} [m^{-2}]	M	q	H [GPa]
0.5	35	0.37	56	13	2.1	0.75	1.98
1	22	0.36	35	33	2.0	0.37	2.23
3	19	0.40	33	42	2.0	0.37	2.74
6	14	0.45	28	30	1.55	0.85	2.57

Table 2.b. The microstructural parameters and the hardness for the samples compacted from the powders with different nominal Mg content milled for 3 h.

Nominal Mg [wt%]	m [nm]	σ	$\langle x \rangle_{vol}$ [nm]	ρ 10^{14} [m^{-2}]	M	q	H [GPa]
0	64	0.24	78	10	1.41	0.99	1.11
3	33	0.30	45	28	2.0	0.83	2.29
6	19	0.40	33	42	2.0	0.37	2.74

The hardness of the compacted samples were measured by depth sensing Vickers indentation. The load was selected to be such small (100 mN) that the diagonals of

indentation patterns (8-15 μm) were about one-tenth of the diameter of the compacted particles. The indentation curves for Al - 6wt% Mg samples milled for up to 6 h are shown in Fig. 7. The indentation curves change significantly with the milling time and this changing correlates to the difference in hardness of materials. The hardness (*H*) was calculated from the maximum load (F_m) and the maximum penetration depth (h_m) by the following formula [25]:

$$H = 0.03784 \cdot F_m / h_m^2 \quad .$$ (8)

The hardness number, *H*, may differ slightly from the value that could be calculated by optical measurement of the indentation due to piling up of the material around the pattern [43]. The hardness was preferred to be determined from the indentation curves against the optical measurement of the pattern because of the higher accuracy of the penetration depth comparing to the indentation diagonal. The hardness values for the compacted specimens are listed in Tables 2.a and 2.b and plotted in Figs. 4 and 5. Each value is obtained as the mean of ten measurements. The relative uncertainty of the hardness is very low, 3 %, due to the high precision of the indentation depth measurement. The hardness determined for pure Al milled for 3 h (1.11 GPa) is in good agreement with the value of 1.27 GPa obtained for Al milled for 10 h by Rodriguez et al. [44]. One can establish that the hardness is increasing with the nominal Mg content of Al alloys. The hardness increment is caused by the increasing of the Mg concentration (solute hardening) and also by the increasing of the dislocation density (work hardening) and even by the decreasing of the crystallite size [38]. The effect of
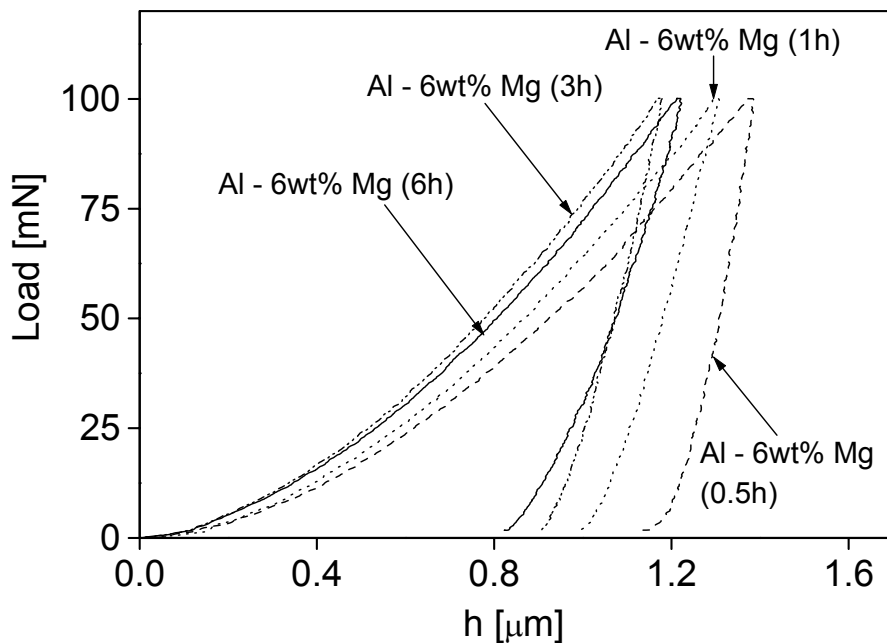

Fig. 7. The indentation curves for Al - 6wt% Mg samples milled for up to 6 h.

the grain size on the hardness of Al - 3% Mg alloy was studied by Furukawa et al. [45]. They have found that the Hall-Petch equation relating the hardness to the grain size is valid for bulk Al - 3% Mg produced by severe plastic deformation with the grain size (d) between 100 nm and 100 μm:

$$HV = H_0 + k d^{-1/2}, \tag{9}$$

where H_0 and k are appropriate constants. For Al - 3% Mg alloys produced by equal channel angular pressing (ECAP) Furukawa and coworkers have obtained H_0=0.46 GPa and k=0.35 GPaμm$^{1/2}$. For Al - 3% Mg fabricated by high pressure torsion straining (HPT) H_0=0.475 GPa and k=0.41 GPaμm$^{1/2}$ have been found [45]. For our ball milled Al - 3wt% Mg (3h) sample with the grain size of 45 nm, *HV*=2.11 GPa and 2.41 GPa are calculated from eq.(9) using the H_0 and k constants values obtained for ECA pressed and the torsion deformed specimens, respectively. These calculated values are very close to the measured one: 2.29 GPa.

Increasing the milling time first the hardness increases due to the decreasing of crystallite size and the rising of the amount of dislocations and the Mg concentration. Increasing the milling time from 3 to 6 h the crystallite size and the Mg content did not change but the dislocation density slightly decreased resulting in a slight decrease of the hardness. The decrease of the dislocation density at large strain values in Al-Mg alloys has been observed for high temperature deformation (305^{0}C) [46]. This effect was explained by the dynamic recovery of the grain interiors [46]. However, it should be noted that the dislocation density values determined by Duly et al. had very large uncertainty [46]. Nevertheless, the decrease of the dislocation density in the sample Al - 6wt% Mg (6h) may be caused by breaking away of the dislocations from their solute-atom atmospheres due to the high stress during milling [47] followed by the annihillation of the mobile edge dislocations. The latter is supported by the changes in the character of dislocations from more edge to mixed one (see Table 1.a). These processes may be caused by warming up of the powder during long milling periods, as mentioned above at the discussion of the evolution of the dislocation structure.

5. CONCLUSIONS

Al-Mg alloys were produced by ball milling of Al and Mg powders. It is shown that alloying and the formation of nanostructures occur simultaneously during the severe plastic deformation. The effect of the nominal Mg powder content and the milling time on the microstructure and the hardness was studied. The crystallite size distribution and the dislocation structure were determined by X-ray diffraction profile analysis while the hardness was obtained from depth sensing Vickers indentation tests.

Increasing the milling time first the hardness increases due to the fast decrease of the crystallite size and the increase of the amount of dislocations and the solute Mg

concentration in the Al matrix. Further increasing the milling time from 3 to 6 h the crystallite size and the Mg content did not change but the dislocation density slightly decreased concomitant with the slight decrease of the hardness. With increasing milling time the character of dislocations is shifted from mixed to more edge type, however, after 6 h milling the character becomes mixed again.

The hardness increased with the nominal Mg content for the same milling time due to the increase of the Mg concentration and the dislocation density and due to the decrease of the crystallite size. With increasing Mg content the dislocation character became gradually more edge type. The hardness obtained for the mechanically alloyed Al - 3wt% Mg specimen agrees well with those predicted from the Hall-Petch relationship determined for bulk samples in previous works.

ACKNOWLEDGEMENTS

REFERENCES

1. L. Lu and Y. F. Zhang, **J. Alloys and Compounds 290** (1999) 279.
2. J.-H. Ahn and Y.-K. Paek, **J. Mater. Sci. Letters 18** (1999) 17.
3. G. B. Schaffer and J. S. Forrester, **J. Mater. Sci. 32** (1997) 3157.
4. J. R. Harris, J. A. D. Wattis and J. V. Wood, **Acta mater. 49** (2001) 3991.
5. H. Huang, J. Pan and P. G. McCormick, **Mat. Sci. Eng. A 232** (1997) 55.
6. G. K. Williamson and W. H. Hall, **Acta Metall. 1** (1953) 22..
7. B. E. Warren and B. L. Averbach, **J. Appl. Phys. 21** (1950) 595.
8. B. E. Warren, Progr. **Metal Phys. 8** (1959) 147.
9. J. I. Langford, D. Louer and P. Scardi, **J. Appl. Cryst. 33** (2000) 964.
10. C. E. Krill and R. Birringer, **Phil. Mag. A 77** (1998) 621.
11. M. Rand, J. I. Langford and J. S. Abell, **Phil. Mag. B 68** (1993) 17.
12. A. J. C. Wilson, **X-ray Optics**, Methuen, London. (1962).
13. J. Gubicza, J. Szépvölgyi, I. Mohai, L. Zsoldos and T. Ungár, **Mat. Sci. Eng. A 280** (2000) 263.
14. G. Caglioti, A. Paoletti and F. P. Ricci, **Nucl. Instrum. 3** (1958) 223.
15. P. Suortti, in The Rietveld Method, edited by R. A. Young, **IUCr Monographs on Crystallography**, Vol. 5., Oxford University Press, (1993) 167.
16. A. Le Bail, Proc. **Accuracy in Powder Diffraction II**, NIST Special Publication, **846** (1992) 142.
17. M. A. Krivoglaz, Theory of X-ray and Thermal Neutron Scattering by Real Crystals,

Plenum Press, N. Y. (1996) and X-ray and Neutron Diffraction in **Nonideal Crystals**, Springer-Verlag, Berlin Heidelberg New York. (1969).

18. M. Wilkens, **phys. stat. sol.** (a) **2** (1970) 359.
19. M. Wilkens, **Fundamental Aspects of Dislocation Theory**, ed. J. A. Simmons, R. de Wit, R. Bullough, Vol. II. Nat. Bur. Stand. (US) Spec. Publ. No. 317, Washington, DC. USA (1970) 1195.
20. P. Klimanek and Jr R. Kuzel, **J. Appl. Cryst**. **21** (1988) 59.
21. T. Ungár and A. Borbély, **Appl. Phys. Lett**. **69** (1996) 3173.
22. P. Scardi and M. Leoni, **J. Appl. Cryst**. **32** (1999) 671.
23. T. Ungár, J. Gubicza, G. Ribárik and A. Borbély, **J. Appl. Cryst**. **34** (2001) 298.
24. G. Ribárik, T. Ungár and J. Gubicza, **J. Appl. Cryst**. **34** (2001) 669.
25. J. Gubicza, A. Juhász and J. Lendvai, **J. Mater. Res**. **11** (1996) 2964.
26. R. Kuzel and P. Klimanek, **J. Appl. Cryst**. **21** (1988) 363.
27. T. Ungár, I. Dragomir, Á. Révész and A. Borbély, **J. Appl. Cryst**. **32** (1999) 992.
28. T. Ungár and G. Tichy, **phys. stat. sol**. (a) **171** (1999) 425.
29. T. Ungár, A. Borbély, G. R. Goren-Muginstein, S.Berger and A. R. Rosen, **Nanostructured Materials 11,** 103 (1999).
30. J. Gubicza, J. Szépvölgyi, I. Mohai, G. Ribárik and T. Ungár, **J. Mat. Sci**. **35** (2000) 3711.
31. W. C. Hinds, **Aerosol Technology: Properties, Behavior and Measurement of Airbone Particles** , Wiley, New York. (1982).
32. A. R. Stokes, **Proc. Phys. Soc.** London **61** (1948) 382.
33. D. M. Pool & H. J. Axon, **J. Inst. Met. 80** (1952) 599.
34. L. F. Mondolfo, **Internat. Metall. Rev. 153** (1971) 95.
35. I. Kovács, J. Lendvai and E. Nagy, **Acta Met. 20** (1972) 975.
36. Á. Révész, J. Lendvai and T.Ungár, **Mat. Sci. Forum 343-346** (2000) 326.
37. R. F. S. Hearmon, **Landolt-Börnstein**, **1** (1966) 1.
38. M. Verdier, I. Groma, L. Flandin, J. Lendvai, Y. Bréchet and P. Guyot, **Scripta Mat. 37** (1997) 449.
39. D. A. Hughes, **Acta metall. mater. 41** (1993) 1421.
40. G. F. Dirras, M.-P. Biget and C. Rey, **Scripta Mat. 33** (1995) 755.
41. D. Kuhlmann-Wilsdorf, **Mat. Sci.Eng.**A **113** (1989) 1.
42. B. Bay, N. Hansen, D. A. Hughes and D. Kuhlmann-Wilsdorf, **Acta metall. mater. 40** (1992) 205.
43. J. Gubicza, N. Rozlosnik and A. Juhász, **J. Mater. Sci. Letters 16** (1997) 1904.
44. J. A. Rodriguez, J. M. Gallardo, E. J. Herrera, **J. Mat. Sci. 32** (1997) 3535.
45. M. Furukawa, Z. Horita, M. Nemoto, R. Z. Valiev and T. G. Langdon, **Acta mater. 44** (1996) 4619.
46. D. Duly, G. J. Baxter, H. R. Shercliff, J. A Whiteman, C. M. Sellars and M. F. Ashby, **Acta mater. 44** (1996) 2947.
47. S. S. Woo, Y. R. Kim, D. H. Shin and W. J. Kim, **Scripta Mater. 37** (1997) 1351.